^{13}C(^{11}B, ^{12}C)^{12}B REACTION AT 45 MeV, ^{12}C + ^{12}B INTERACTION VERSUS THAT OF ^{12}C + ^{10,11}B

S.Yu. Mezhevych[a], A.T. Rudchik[a], A.A. Rudchik[a]
K.W. Kemper[b], K. Rusek[c], O.A. Ponkratenko[a], E.I. Koshchy[d]
S.B. Sakuta[e]

[a]Institute for Nuclear Research, Ukrainian Academy of Sciences
Prospect Nauki 47, 03680 Kyiv, Ukraine
[b]Physics Department, Florida State University, Tallahassee, FL 32306-4350, USA
[c]Heavy Ion Laboratory, University of Warsaw
Pasteura 5A, 02-093 Warsaw, Poland
[d]Cyclotron Institute Texas A&M University, College Station, TX 77843, USA
[e]Russian Research Center "Kurchatov Institute"
Kurchatov Sq. 1, 123182 Moscow, Russia

(Received June 18, 2020; accepted August 20, 2020)

Complete angular distributions including both forward and backward angles are reported for the reaction ^{13}C(^{11}B, ^{12}C)^{12}B at $E_{\rm lab}(^{11}\mathrm{B}) = 45$ MeV leading to the ground and excited states of ^{12}C and ^{12}B. This reaction explores the interplay of proton and neutron transfers as well of those for larger clusters. The experimental data were analyzed within the coupled-reaction-channels method (CRC) that included the $^{13}\mathrm{C}+^{11}\mathrm{B}$ elastic scattering channel as well as channels for one- and two-step transfers of nucleons in the coupling scheme. The necessary $^{13}\mathrm{C}+^{11}\mathrm{B}$ optical potential parameters were obtained from previous work, while those for $^{12}\mathrm{C} + ^{12}\mathrm{B}$ were deduced from fitting the calculations to the ^{13}C(^{11}B, ^{12}C)^{12}B reaction data. Needed spectroscopic amplitudes of transferred nucleons and clusters were calculated within the translational-invariant shell model (TISM). The data are well-described by proton transfers while contributions from neutron transfer are only important at the largest angles. New global optical potentials for the elastic scattering of ^{8,10,11}B isotopes were tested and found to describe the forward angles reaction data but not those for the middle and larger angles even when the ground-state reorientation of ^{11}B in the entrance channel is included.

DOI:10.5506/APhysPolB.51.1949

1. Introduction

The interaction between similar mass light nuclei has led to a greater understanding of the impact of inelastic scattering and transfer reactions on the measured elastic scattering angular distribution. This sensitivity of contributions to the scattering from processes other than pure potential scattering has been most clearly seen in the large angle data of the interacting systems. For example, the large angle elastic scattering data of the system $^{12}\mathrm{C} + {}^{11}\mathrm{B}$ has contributions from proton transfer and ^{11}B ground-state reorientation, giving rise to a much larger cross section than expected [1]. In the case of $^{13}\mathrm{C} + {}^{11}\mathrm{B}$, potential scattering gives large angle predictions that are oscillatory, with the ^{11}B ground-state reorientation being less, so resulting in the structureless data being well-described by the two contributions [2]. This difference can be seen directly from the data with the $^{12}\mathrm{C} + {}^{11}\mathrm{B}$ large angle cross section being an order of magnitude larger than that for $^{13}\mathrm{C} + {}^{11}\mathrm{B}$. The present full angular range data set for the reaction $^{13}\mathrm{C}(^{11}\mathrm{B}, {}^{12}\mathrm{C})^{12}\mathrm{B}$ at $E_{\mathrm{lab}}(^{11}\mathrm{B}) = 45$ MeV furthers these studies because it is sensitive to both contributions from proton and neutron transfers as well as the exit channel $^{12}\mathrm{C} + {}^{12}\mathrm{B}$ optical potential. In addition, the magnitude and shape of the reaction data tests the spectroscopic amplitudes for various underlying transfers between the interacting partners and gives further details of the structure of ^{12}B. Moreover, these new data provide a test of recently published global phenomenological optical model (OM) potentials for ^{8,10,11}B projectiles [3] since they provide the entrance and exit channel potentials needed in the Coupled Reaction Channels (CRC) analysis of this reaction.

Only limited data has been taken so far with ^{12}B beams since it must be produced as a secondary beam thus limiting its intensity. Elastic scattering data from a ^{58}Ni [4] target with the purpose of investigating its optical potential has been measured. A secondary beam was also used in scattering by protons [5] to search for the excited $T = 3/2$ states in the $A = 13$ nuclei chain. More recent interest in the structure of ^{12}B has been stimulated by the possibility that its excited states could be considered to have halo structure, leading to an analysis of the $^{11}\mathrm{B}(d, p)^{12}\mathrm{B}$ reaction to determine the root-mean-square (RMS) radii of its states as well as spectroscopic factors and asymptotic normalization coefficients (ANC) [6]. In other studies, the cluster structure of ^{12}B was probed with reactions such as $^{14}\mathrm{C}(d, \alpha)$ [7], $^{8}\mathrm{Li} + {}^{4}\mathrm{He}$ [8], $^{7}\mathrm{Li} + {}^{7}\mathrm{Li}$ [9], $^{7}\mathrm{Li} + {}^{9}\mathrm{Be}$ [10] that produced ^{12}B in their exit channels. Further study of the spectroscopic properties of ^{12}B and ^{13}B nuclei for possible astrophysical implications were reported in Refs. [11, 12] through the reactions $^{11}\mathrm{B}(d, p)^{12}\mathrm{B}$ and $d(^{12}\mathrm{B}, p)^{13}\mathrm{B}$. In addition, the charge-exchange reaction $^{12}\mathrm{C}(^{7}\mathrm{Li}, {}^{7}\mathrm{Be})^{12}\mathrm{B}$ [13] was used for the study of ^{12}B.

The paper is organized as follows. Section 2 contains a brief description of the experimental method, Section 3 the procedure for the CRC-calculations, tables with the deduced optical potential parameters for the entrance $^{13}C + ^{11}B$ and exit $^{12}C + ^{12}B$ channels, the spectroscopic amplitudes of the transferred nucleons and clusters, and the results of the reaction analysis. The last section provides the summary of this work.

2. Experimental procedure

Angular distributions of the $^{13}C(^{11}B, X)$ scattering and transfer reactions were measured simultaneously at the energy $E_{lab}(^{11}B) = 45$ MeV using the ^{11}B beam from the Warsaw University cyclotron U-200P. The experimental system and data analysis have been described in several previous publications [2,14] without the detailed information about some methods used to obtain the experimental spectra for isotopes from the measured two-dimentional Z-spectra.

In the present work, we used the following method to extract the experimental data of the reaction $^{13}C(^{11}B, ^{12}C)^{12}B$: loci for carbon and boron isotopes, resolved by the ionization chamber serving as the ΔE dectector in the experiment [2], were devided into sub-loci for ^{12}C, ^{13}C, ^{14}C and ^{10}B, ^{11}B, ^{12}B isotopes, as shown in Fig. 1(a) and (d), respectively, assuming the width of each sub-locus equal to the ΔE width of prominent peaks for ^{13}C and ^{11}B in the ground states from the elastic scattering, well-separated from the rest of the reaction products. The resulting spectra for ^{12}C and ^{12}B, extracted in this way, are shown in Fig. 1(b) and (e), respectively. The continuous energy contributions from multi-particle reaction products, overlaps from the neighbouring sub-loci and reaction products from ^{12}C impurities in the target were approximated by the background functions of the form of

$$N_{bg}(E) = \sum_i N_{0i} \left[1 + \exp\left(-\frac{E - E_{1i} + E_{2i}/2}{H_{1i}}\right)\right]^{-1} \times \left\{1 - \left[1 + \exp\left(-\frac{E - E_{1i} - E_{2i}/2}{H_{2i}}\right)\right]^{-1}\right\} \quad (1)$$

with fitting parameters N_{0i}, E_{1i}, E_{2i}, H_{1i} and H_{2i} $(i = 1, 2, ..., m)$ to determine the spectrum minima, choosing the necessary number of these functions$m$, by means of the computer code PeakFit. These background functions are shown in Fig. 1(b) and (e) by the solid curves.

The contributions of ^{12}C from the reaction $^{12}C(^{11}B, ^{12}C)^{11}B$ were estimated using the data of previously studied elastic and inelastic scattering $^{12}C + ^{11}B$ at the energy $E_{lab}(^{11}B) = 49$ MeV [1] measured on the same experimental setup. These contributions are shown in Fig. 1(b) by the dashed

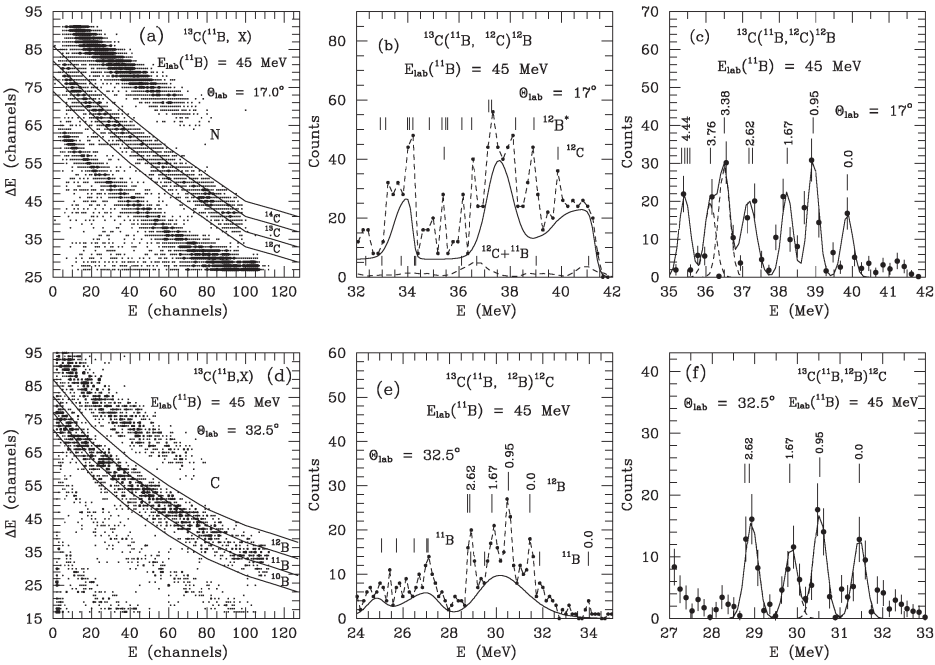

Fig. 1. Typical ΔE–E spectra for carbon (a) and boron (d) isotopes from the reaction ^{13}C(^{11}B, ^{12}C)^{12}B at $E_{\rm lab}(^{11}{\rm B}) = 45$ MeV and energy spectra of ^{12}C and ^{12}B with backgrounds (b), (e) (curves show background forms) and (c), (f) after subtraction of the backgrounds (curves show the Gauss symmetric fitted forms). See also the text for detailed explanation.

curve. The contributions of the ^{12}B products from the ^{12}C(^{11}B, ^{12}B)^{11}C reaction are absent in Fig. 1(e) because the Q-value of this reaction is -15.36 MeV.

The energy spectra of ^{12}C and ^{12}B obtained after the subtractions of the backgrounds are shown in Fig. 1(c) and (f), respectively. The peaks of experimental residual energy spectra were approximated with the symmetric Gaussian functions. Since these spectra still contain residual backgrounds of different sources such as overlaps from poorly resolved energy peaks, possible noises of electronic equipment *etc.*, we used the following procedure to minimize the influence of these residual backgrounds on the extracted peak areas: the width of Gaussian functions was taken from the fit of well-resolved peaks and applied as fixed to all other peaks in the residual energy spectra. In this way, the areas under the peaks of the residual ^{12}C and ^{12}B spectra were used for the calculation of the angular distributions at the angles $\theta_{\rm cm}(^{12}{\rm C})$ and $\theta_{\rm cm}(^{12}{\rm C}) = 180° - \theta_{\rm cm}(^{12}{\rm B})$, respectively. In this way, the angular distributions of the ^{13}C(^{11}B, ^{12}C)^{12}B reaction were determined over

the whole angular range. The area errors of the peaks were estimated to be about 20%, if the peaks were well resolved and 30–40% for poorly resolved peaks.

The obtained angular distributions of the ^{13}C(^{11}B, ^{12}C)^{12}B reaction were normalized using the normalization factor the same as for the ^{13}C + ^{11}B elastic and inelastic scattering measured in the same experiment [2].

3. Analysis of the reaction data

The ^{13}C(^{11}B, ^{12}C)^{12}B experimental data were analyzed within the CRC method. The ^{13}C + ^{11}B elastic and inelastic scattering channels as well as transfer reactions, shown on diagrams in Fig. 2, were included in the channel coupling scheme. Standard Woods–Saxon (WS) optical potentials were used in entrance and exit channels of the calculations and their form, given here for completeness, is

$$U(r) = V_0 \left[1 + \exp\left(\frac{r - R_V}{a_V}\right)\right]^{-1} + iW_S \left[1 + \exp\left(\frac{r - R_W}{a_W}\right)\right]^{-1} \tag{2}$$

with the Coulomb potential being that for uniformly charged spheres

$$V_C(r) = \begin{cases} \frac{Z_P Z_T e^2}{2R_C}\left(3 - \frac{r^2}{R_C^2}\right), & r \le R_C \\ \frac{Z_P Z_T e^2}{r}, & r > R_C \end{cases} . \tag{3}$$

Here, the form of the radii is given by

$$R_i = r_i \left(A_P^{1/3} + A_T^{1/3}\right), \qquad i = V, W, C, \tag{4}$$

where A_P, A_T and Z_P, Z_T are the mass and charge numbers of ^{11}B, ^{13}C (entrance channel) and ^{12}C, ^{12}B (exit channel). The parameter $r_C = 1.25$ fm was used in all the calculations.

The wave function of x for a nucleus $A = C + x$ was calculated by varying the depth of the Woods–Saxon binding potential to reproduce the binding energy of nucleus A. The geometry parameters of the cluster binding potentials were the following: $a = 0.65$ fm and $r_0 = 1.25A^{1/3}/(C^{1/3} + x^{1/3})$ fm.

The calculations were performed by means of the code Fresco [15]. For the entrance ^{13}C + ^{11}B channel, the WS-potential parameters were taken from Ref. [2], in which the elastic and inelastic scattering of these nuclei was investigated. The parameters of the WS potential for the ^{12}C + ^{12}B interaction were deduced from the fit of the calculated cross sections to the ^{13}C(^{11}B, ^{12}C)^{12}B experimental data with the final parameters of the WS potentials given in Table I.

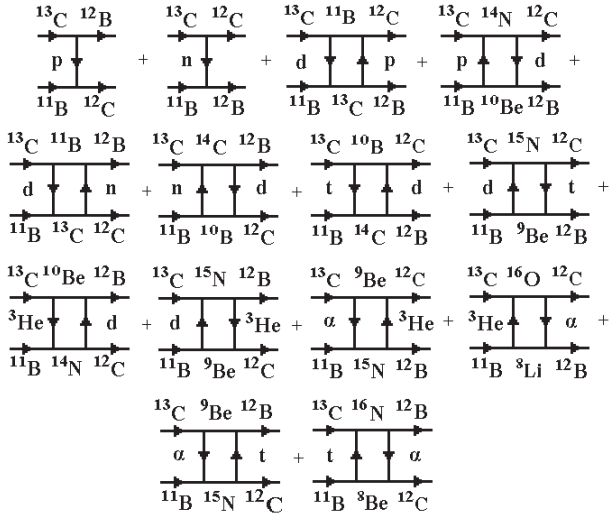

Fig. 2. Diagrams of different ^{13}C(^{11}B, ^{12}C)^{12}B reaction mechanisms.

TABLE I

Parameters of WS optical potentials.

T+P	$E_{\rm cm}$ [MeV]	V_0 [MeV]	r_V [fm]	a_V [fm]	W_S [MeV]	r_W [fm]	a_W [fm]	Ref.
^{13}C + ^{11}B	24.38	256.7	0.788	0.740	7.0	1.250	0.740	[2]
^{12}C + ^{12}B	22.80	177.0	0.788	0.740	9.0	1.000	0.600	This work
^{12}C + ^{11}B	22.17	251.0	0.788	0.670	8.0	1.250	0.670	[1]
^{12}C + ^{10}B	22.53	100.0	1.150	0.428	15.0	1.300	0.248	[20]

Spectroscopic amplitudes S_x of clusters x for the nuclear systems $A = C + x$, used in the calculations, were obtained within the translational invariant shell model (TISM) [16] using the computer code DESNA [17, 18] and Boyarkina's wave function tables for 1p-shell nuclei [19]. The calculated values of the amplitudes S_x are listed in Table II.

Angular distributions of the reaction ^{13}C(^{11}B, ^{12}C)^{12}B at $E_{\rm lab}(^{11}{\rm B}) = 45$ MeV for the ground states of ^{12}C and ^{12}B are shown in Fig. 3 together with the results of the calculations for different transfer reactions. Proton transfer (curve $\langle p \rangle$) dominates the reaction ^{13}C(^{11}B, ^{12}C)^{12}B at $E_{\rm lab}(^{11}{\rm B}) = 45$ MeV at all angles which is consistent with expectations based on the large $^{11}{\rm B} + p \to {}^{12}{\rm C}$ spectroscopic amplitude listed in Table II. Neutron transfer (curve $\langle n \rangle$) contributes only at the most backward angles. The contributions

TABLE II

Spectroscopic amplitudes S_x of x-clusters in $A = C + x$ systems.

A	C	x	nL_j	S_x	A	C	x	nL_j	S_x
^{11}B	^{8}Li	^{3}He	$2P_{1/2}$	0.160[a]	$^{12}B^{*}_{2.62}$	^{11}B	n	$2S_{1/2}$	− 0.142[a]
			$1F_{5/2}$	0.218[a]				$1D_{3/2}$	− 0.127
			$1F_{7/2}$	0.214	$^{12}B^{*}_{2.72}$	^{11}B	n	$1P_{3/2}$	0.478
^{11}B	^{8}Be	t	$2P_{3/2}$	0.641	^{12}C	^{8}Be	α	$3S_0$	0.822
^{11}B	^{9}Be	d	$2S_1$	− 0.607[a]	^{12}C	^{9}Be	^{3}He	$2P_{3/2}$	1.224[a]
			$1D_1$	− 0.109[a]	^{12}C	^{10}B	d	$1D_3$	1.780
			$1D_3$	0.610[a]	^{12}C	^{11}B	p	$1P_{3/2}$	− 1.706[a]
^{11}B	^{10}Be	p	$1P_{3/2}$	0.699	^{13}C	^{9}Be	α	$2D_2$	0.504[a]
^{11}B	^{10}B	n	$1P_{3/2}$	− 1.347[a]	^{13}C	^{10}Be	^{3}He	$2P_{1/2}$	0.170
^{12}B	^{8}Li	α	$2D_2$	0.496[a]	^{13}C	^{10}B	t	$1F_{5/2}$	0.109[a]
$^{12}B^{*}_{0.95}$	^{8}Li	α	$3S_0$	− 0.411				$1F_{7/2}$	0.747
			$2D_2$	− 0.325	^{13}C	^{11}B	d	$2S_1$	− 0.263
			$1G_4$	0.205				$1D_1$	− 0.162
$^{12}B^{*}_{1.67}$	^{8}Li	α	$3P_1$	− 0.411[a]				$1D_2$	− 0.485[a]
			$2F_3$	− 0.325[a]	^{13}C	^{12}B	p	$1P_{1/2}$	− 0.694[a]
^{12}B	^{9}Be	t	$2P_{1/2}$	0.102[a]				$1P_{3/2}$	0.245
			$2P_{3/2}$	0.091	^{13}C	$^{12}B^{*}_{0.95}$	p	$1P_{3/2}$	− 0.736[a]
			$1F_{5/2}$	0.512[a]	^{13}C	$^{12}B^{*}_{1.67}$	p	$1D_{3/2}$	− 0.736[a]
$^{12}B^{*}_{0.95}$	^{9}Be	t	$2P_{1/2}$	− 0.237	^{13}C	$^{12}B^{*}_{2.62}$	p	$1S_{1/2}$	− 0.694[a]
			$1F_{5/2}$	− 0.323				$1D_{3/2}$	0.245
			$1F_{7/2}$	0.316[a]	^{13}C	$^{12}B^{*}_{2.72}$	p	$1P_{1/2}$	− 0.375
$^{12}B^{*}_{1.67}$	^{9}Be	t	$3S_{1/2}$	− 0.237	^{13}C	$^{12}B^{*}_{3.39}$	p	$1D_{5/2}$	− 0.628
			$1G_{5/2}$	− 0.323	^{13}C	$^{12}B^{*}_{3.76}$	p	$1P_{3/2}$	− 0.601[a]
			$1G_{7/2}$	0.316[a]	^{13}C	^{12}C	n	$1P_{1/2}$	0.601
^{12}B	^{10}Be	d	$1D_1$	0.380	^{14}C	^{11}B	t	$2P_{3/2}$	− 0.368[a]
$^{12}B^{*}_{0.95}$	^{10}Be	d	$1D_2$	0.380	^{14}C	^{12}B	d	$1D_1$	− 1.010
$^{12}B^{*}_{1.67}$	^{10}Be	d	$1P_2$	0.380	^{14}C	$^{12}B^{*}_{0.95}$	d	$1D_2$	− 1.304
^{12}B	^{11}B	n	$1P_{1/2}$	− 0.142	^{14}C	$^{12}B^{*}_{1.67}$	d	$1P_2$	− 1.304
			$1P_{3/2}$	− 0.127[a]	^{14}C	^{13}C	n	$1P_{1/2}$	− 1.094[a]
$^{12}B^{*}_{0.95}$	^{11}B	n	$1P_{1/2}$	0.270	^{14}N	^{11}B	^{3}He	$2P_{1/2}$	− 0.107[a]
			$1P_{3/2}$	0.270[a]				$2P_{3/2}$	− 0.096
$^{12}B^{*}_{1.67}$	^{11}B	n	$2S_{1/2}$	0.330				$1F_{5/2}$	− 0.292[a]
^{14}N	^{12}C	d	$1D_1$	0.246	^{15}N	^{13}C	d	$2S_1$	0.248[a]
^{14}N	^{13}C	p	$1P_{1/2}$	0.461				$1D_1$	0.444[a]
			$1P_{3/2}$	0.163[a]	^{16}N	^{12}B	α	$4P_1$	− 0.384
^{15}N	^{11}B	α	$2D_2$	0.435[a]	^{16}N	$^{12}B^{*}_{0.95}$	α	$3P_1$	− 0.411[a]
^{15}N	^{12}B	^{3}He	$2P_{1/2}$	0.254[a]				$2F_3$	− 0.325[a]
			$2P_{3/2}$	− 0.090	^{16}N	$^{12}B^{*}_{1.67}$	α	$3S_0$	− 0.411
^{15}N	$^{12}B^{*}_{0.95}$	^{3}He	$2P_{3/2}$	0.269[a]	^{16}N	^{13}C	t	$2D_{3/2}$	− 0.194
			$1F_{5/2}$	− 0.274	^{16}O	^{12}C	α	$3S_0$	0.544
^{15}N	$^{12}B^{*}_{1.67}$	^{3}He	$2D_{3/2}$	0.269[a]	^{16}O	^{13}C	^{3}He	$2P_{1/2}$	0.910[a]
^{15}N	^{12}C	t	$2P_{1/2}$	0.380					

[a] $S_{\mathsf{Fresco}} = (-1)^{J_C+j-J_A} S_x = -S_x$.

of two-step transfers of $d+n$ and $n+d$ (curve $\langle dn\rangle$, coherent sum), $d+t$ and $t+d$ (curve $\langle dt\rangle$), $d+p$ and $p+d$ (curve $\langle dp\rangle$), $\alpha+t$ and $t+\alpha$ (curve $\langle \alpha t\rangle$), α + ^{3}He and ^{3}He$+\alpha$ (curve $\langle \alpha^3\mathrm{He}\rangle$), $d+^3$He and ^{3}He$+d$ (curve$\langle d^3\mathrm{He}\rangle$) are not significant. The solid curve $\langle \Sigma\rangle$ shows the coherent sum of all included transfer reactions.

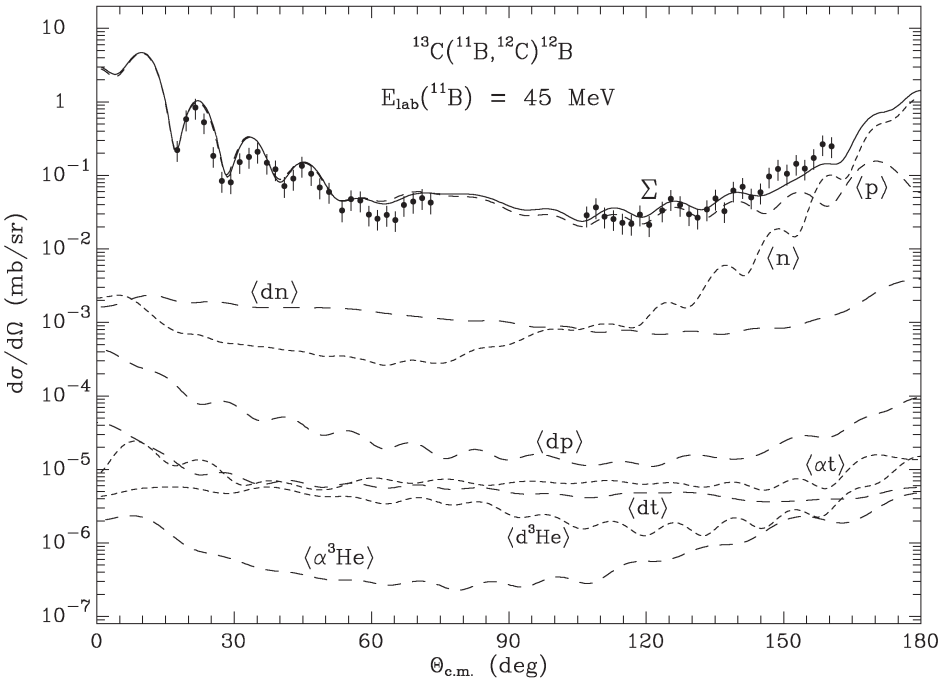

Fig. 3. Angular distribution of the ^{13}C(^{11}B, ^{12}C)^{12}B reaction at the energy of $E_{\mathrm{lab}}(^{11}\mathrm{B}) = 45$ MeV leading to the ground state of ^{12}B. The curves show cross sections calculated with the WS potentials (Table I) for different transfer processes.

In Fig. 4, we show the comparison of the sums $\langle\Sigma\rangle$ of the calculated cross sections using the OM parameters obtained in this work for the ^{12}C + ^{12}B elastic scattering, and the parameters for ^{12}C + ^{11}B [1] and ^{12}C + ^{10}B [20] interactions (see Table I). At far forward angles, the different potential sets give almost the same reaction cross sections but visible differences for the reaction appear in the middle-angle region when the ^{12}C + ^{11}B [1] and ^{12}C + ^{10}B [20] potentials are used. This is the *isotopic effect* that originates from the structural differences in the ^{10,11,12}B isotopes. For example, it has been known for many years that non-central potential contributions arise in the scattering of ^{10}B nuclei from its large ground-state quadrupole moment.

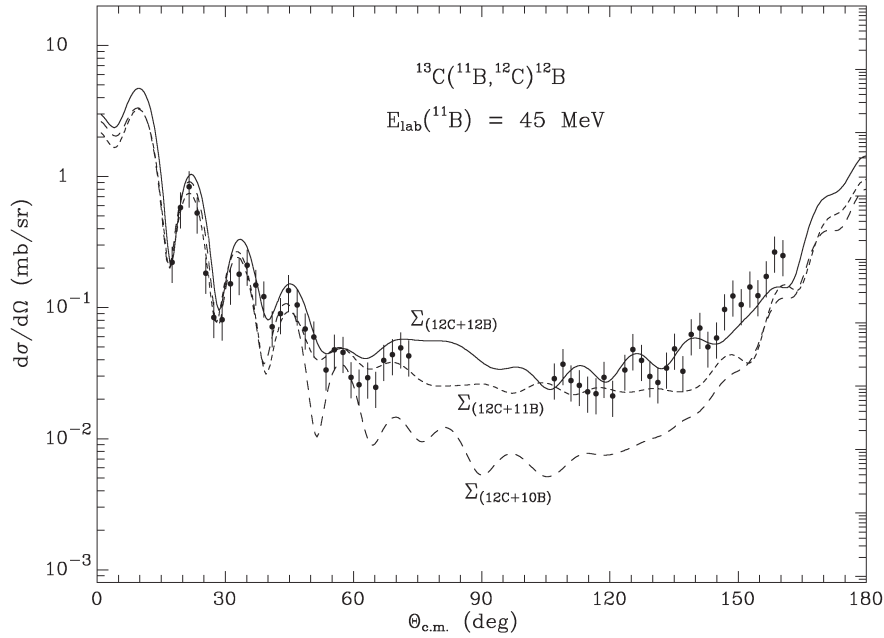

Fig. 4. Angular distributions of the $^{13}C(^{11}B, ^{12}C)^{12}B$ reaction for the ground states of ^{12}C and ^{12}B. The curves show CRC calculations with different OM parameters for the $^{12}C + ^{12}B$ interaction (Table I).

Angular distributions of the reaction for transitions to the excited states 0.953 MeV (2^+) and 1.674 MeV (2^-) of ^{12}B are shown in Fig. 5 together with CRC calculations. Curves $\langle p \rangle$ and $\langle n \rangle$ show contributions of proton and neutron transfers, respectively, and the curves Σ_{2st} show the coherent sums of the two-step processes. Solid curves $\langle \Sigma \rangle$ show the coherent sums of one- and two-step processes. As can be seen, the contributions of two-step processes are negligible for the excited states of ^{12}B, as proton and neutron transfers dominate.

Angular distributions and results of the calculations for transitions to the excited states 2.62 MeV (1^-) and 2.72 MeV (0^+) of ^{12}B (unresolved in the experiment) are shown in Fig. 6. The dashed curves $\Sigma_{2.62}$ and $\Sigma_{2.72}$ show the coherent sums of calculated cross sections for proton and neutron transfers leading to the excited states 2.62 MeV (1^-) and 2.72 MeV (0^+) of ^{12}B. The solid curve Σ shows the incoherent sum of these two curves. As can be seen, the transfer to the excited state 2.62 MeV (1^-) is dominant in this incoherent sum of the reaction cross sections.

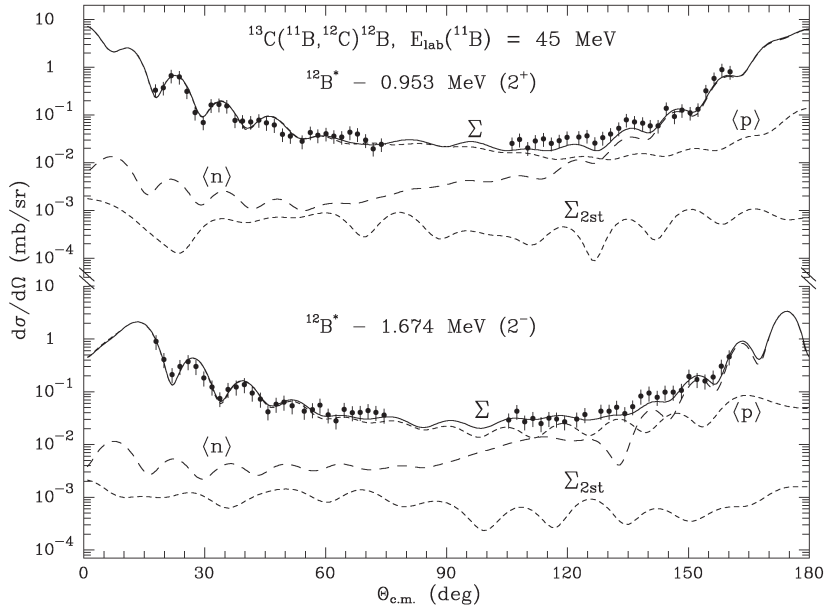

Fig. 5. Angular distributions of the ^{13}C(^{11}B, ^{12}C)^{12}B reaction for transitions to the excited states 0.953 MeV (2^{+}) and 1.674 MeV (2^{-}) of ^{12}B. The curves show results of calculations for different transfer reactions (see the text for details).

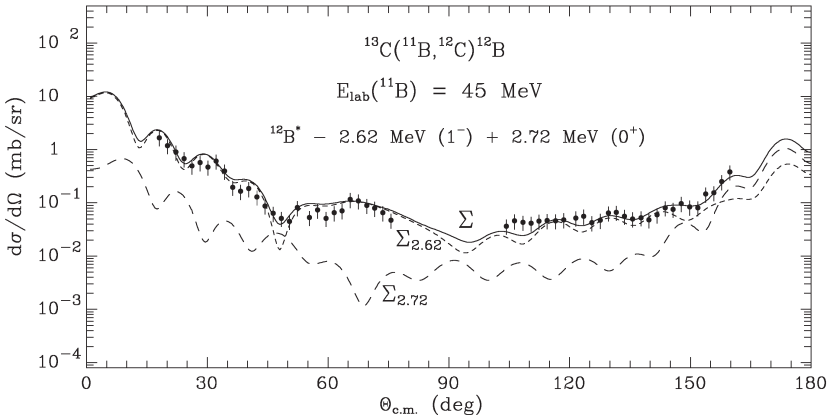

Fig. 6. Angular distributions of the ^{13}C(^{11}B, ^{12}C)^{12}B reaction for transitions to the excited states 2.62 MeV (1^{-}) and 2.72 MeV (0^{+}) of ^{12}B (unresolved in the experiment). The curves show calculated cross sections for different processes (see the text for details). Note that the transition to the 2.62 MeV (1^{-}) state dominates.

The experimental data and results of calculations for transitions to the excited states 3.388 MeV (3^-) and 3.76 MeV (2^+) of ^{12}B are shown in Fig. 7. No large angle data occur here because the ^{12}B nuclei that allow these data to be obtained are unbound and hence undetected. The curves $\langle p \rangle$ show calculated cross sections for the proton transfer.

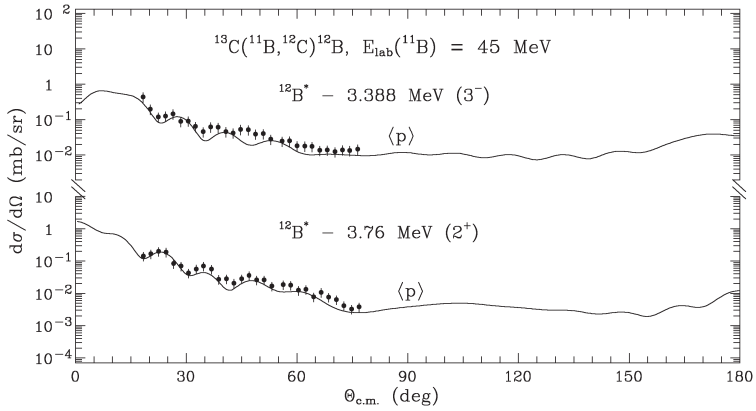

Fig. 7. Angular distributions of the ^{13}C(^{11}B, ^{12}C)^{12}B reaction for transitions to the excited states 3.388 MeV (3^-) and 3.76 MeV (2^+) of ^{12}B. The curves show calculated cross sections for proton transfer process.

The present data allow the test of recently published global optical potentials for ^{8,10,11}B projectiles [3]. The standard global phenomenological OMP in Ref. [3] is defined by

$$V(r,E) = V_0(r,E) + i[W_S(r,E) + W_D(r,E)] + V_C(r)\,. \tag{5}$$

The Coulomb interaction $V_C(r)$ is given by equation (3), the sum of the potentials for the real $V_0(r)$ and imaginary parts for volume absorption $W_S(r)$, adjusted for a given energy E, is defined by equation (2), while the surface imaginary potential $W_D(r)$, adjusted for a given energy E, is given by the expression

$$W_D(r) = 4W_D \left[\exp\left(\frac{r-R_D}{a_D}\right)\right] \Big/ \left[1+\exp\left(\frac{r-R_D}{a_D}\right)\right]^2 . \tag{6}$$

The radii of these potentials are dependent on the target masses only

$$R_i = r_i A_T^{1/3} (i = V, W, D, C)\,. \tag{7}$$

The parameters of the potentials for ^{13}C + ^{11}B and ^{12}C + ^{12}B interaction, taken from global systematics [3] and used in our calculations, are listed in Table III.

TABLE III

Global parameters of WS optical potentials.

T+P	V_0 [MeV]	r_V [fm]	a_V [fm]	W_S [MeV]	r_W [fm]	a_W [fm]	W_D [MeV]	r_D [fm]	a_D [fm]	Ref.
^{13}C + ^{11}B	179.3	1.238	0.852	24.9	1.593	0.598	34.9	1.182	0.869	[3]
^{12}C + ^{12}B	179.1	1.238	0.852	25.1	1.593	0.598	34.8	1.182	0.869	[3]

The calculated angular distribution of the ^{13}C(^{11}B, ^{12}C)^{12}B reaction, assuming coherent sum of proton and neutron transfers (main processes in this reaction), with the global potential parameters [3] (Table III) for the entrance and exit channels, are shown in Fig. 8 by dashed curve. The solid curve shows the calculations with the ^{13}C + ^{11}B potential parameters from Ref. [2] (Table I) and the global ^{12}C + ^{12}B potential parameters (Table III). This latter combination gives a reasonable description of the forward angle data.

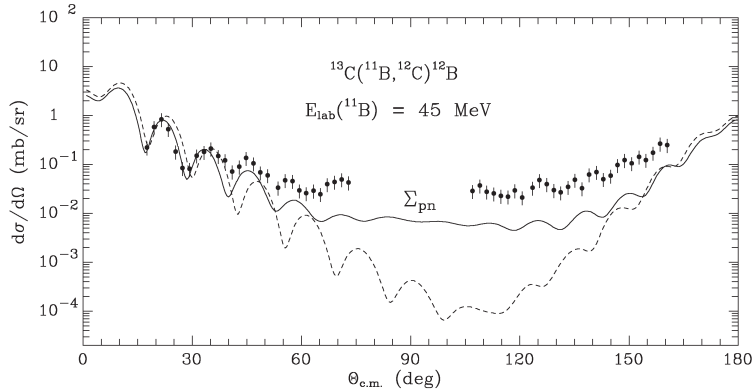

Fig. 8. Angular distributions of the ^{13}C(^{11}B, ^{12}C)^{12}B reaction for the ground states of ^{12}C and ^{12}B. CRC cross sections for coherent sums of proton and neuteron transfers are shown: the dashed curve was calculated with OM potential parameters for the entrance and exit channels from Table III, while the solid curve was calculated with OM potential parameters taken from Table I for the entrance channel and from Table III for the exit channel.

To determine if the large observed difference between the experimental data and calculated cross sections in the middle-angle region was caused by possible strong ground-state reorientation of ^{11}B during the scattering, as suggested by the authors of reference [3], we repeated calculations for the

$^{11}B + ^{13}C$ elastic scattering at $E_{lab}(^{11}B) = 45$ MeV [2] using the OM potential from the global systematics [3] with and without ^{11}B ground-state reorientation: the long-dashed curve in Fig. 9 shows the potential scattering cross sections — it is the same as in Fig. 20 of Ref. [3]. As can be seen, the inclusion of ^{11}B reorientation does not change significantly the resulting CRC cross sections as shown by the solid curve in Fig. 9. From these results, we suggest that either the global phenomenological OM potential proposed in Ref. [3] is more suitable for the prediction of cross sections for the interaction of $^{8,10,11}B$ projectiles with heavier targets ($A > 28$), since the experimental data for these heavier targets were reproduced much better than for lighter targets, or that this global OM potential should be different for ^{12}B projectiles. In order to test the possibility of using the global OM potential [3] for unstable ^{12}B projectiles, more experimental data are needed for the elastic scattering of radioactive ^{12}B nuclei from different light and heavier targets [4].

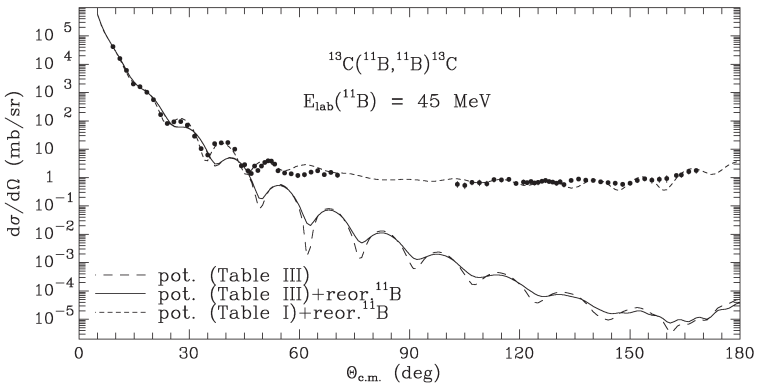

Fig. 9. Angular distributions for $^{13}C(^{11}B, ^{11}B)^{13}C$ elastic scattering. The curves show cross sections calculated with different OM parameters, with and without inclusion of ^{11}B ground-state reorientation.

4. Summary and conclusions

New experimental data (differential cross sections) for the reaction $^{13}C(^{11}B, ^{12}C)^{12}B$ at $E_{lab}(^{11}B) = 45$ MeV leading to the ^{12}B ground state and to excited states between 0.953–3.76 MeV were obtained. The experimental data were analysed within the coupled-reaction-channels (CRC) method that included elastic scattering of $^{11}B + ^{13}C$ as well as one- and two-step transfer reactions in the coupling scheme.

For the entrance reaction channel, a Woods–Saxon (WS) potential was used with the parameters deduced from a previous analysis of the $^{11}B + ^{13}C$ elastic scattering data at $E_{lab}(^{11}B) = 45$ MeV [2]. Spectroscopic ampli-

tudes for nucleons and clusters, needed for the calculations of the reaction cross sections, were obtained within the translational invariant shell model (TISM) [16] by means of the computer code DESNA [18]. The spectroscopic factors of nucleons and clusters in nuclei are defined by the squares of these spectroscopic amplitudes.

The present analysis of the ^{13}C(^{11}B, ^{12}C)^{12}B experimental data found that proton transfer dominates over the whole angular range, with neutron transfers contributing at the largest angles. Contributions of two-step transfers of nucleons and clusters to the ^{13}C(^{11}B, ^{12}C)^{12}B reaction cross sections are negligible.

Comparison of the parameters of WS potentials for the interaction of ^{12}C + ^{12}B, ^{12}C + ^{11}B [1] and ^{12}C + ^{10}B [20] as well as comparison of calculated cross sections for the reaction ^{13}C(^{11}B, ^{12}C)^{12}B with the use of these potentials (in the exit reaction channel) was performed. Differences of these cross sections were observed mainly in the middle-angle region.

Moreover, the experimental data for the reaction ^{13}C(^{11}B, ^{12}C)^{12}B at $E_{\rm lab}(^{11}\mathrm{B}) = 45$ MeV could not be reproduced in the middle and backward-angle regions by calculations using the parameters of the global phenomenological OM potential for ^{8,10,11}B projectiles proposed in Ref. [3], suggesting that, in order to test the validity of this global OM potential [3] for ^{12}B, more experimental data are needed for ^{12}B elastic scattering from a wide range of light and heavy targets.

REFERENCES

[1] A.T. Rudchik *et al.*, «The ^{11}B+^{12}C elastic and inelastic scattering at $E_{\rm lab}(^{11}\mathrm{B}) = 49$ MeV and energy dependence of the ^{11}B + ^{12}C interaction», *Nucl. Phys. A* **695**, 51 (2001).

[2] S.Yu. Mezhevych *et al.*, «The ^{13}C + ^{11}B elastic and inelastic scattering and isotopic effects in the ^{12,13}C + ^{11}B scattering», *Nucl. Phys. A* **724**, 29 (2003).

[3] Y.L. Xu, H.R. Guo, Y.L. Han, Q.B. Shen, «Global phenomenological optical model potentials for ^{8,10,11}B projectiles», *Int. J. Mod. Phys. E* **27**, 1850099 (2019).

[4] E.O.N. Zevallos *et al.*, «Elastic scattering of the ^{12}B + ^{58}Ni system at near-barrier energies», *Phys. Rev. C* **99**, 064613 (2019).

[5] B.B. Skorodunov *et al.*, «$T = 3/2$ states in ^{13}C», *Phys. Rev. C* **78**, 044603 (2008).

[6] T.L. Belyaeva *et al.*, «Neutron halos in the excited states of ^{12}B», *Phys. Rev. C* **98**, 034602 (2018).

[7] A.H. Wuosmaa *et al.*, «Stretched states in ^{12,13}B with the (d, α) reaction», *Phys. Rev. C* **90**, 061301 (2014).

[8] D. Torresi *et al.*, «Li–α cluster states in ^{12}B using $^{8}\mathrm{Li} + {}^{4}\mathrm{He}$ inverse kinematics elastic scattering», *Int. J. Mod. Phys. E* **20**, 1026 (2011).

[9] N. Curtis *et al.*, «$\alpha + \mathrm{Li}$ and $\mathrm{H} + \mathrm{Be}$ decay of ^{10,11,12}B», *Phys. Rev. C* **72**, 044320 (2005).

[10] N. Soic *et al.*, «$^{8}\mathrm{Li} + \alpha$ decay of ^{12}B and its possible astrophysical implications», *Europhys. Lett.* **63**, 524 (2003).

[11] Z.H. Liu *et al.*, «Asymptotic normalization coefficients and neutron halo of the excited states in ^{12}B and ^{13}C», *Phys. Rev. C* **64**, 034312 (2001).

[12] H.Y. Lee *et al.*, «Experimental study of the ^{11}B, $^{12}\mathrm{B}(n,\gamma)$ reactions and their influence on r-process nucleosynthesis of light elements», *Phys. Rev. C* **81**, 015802 (2010).

[13] S.B. Sakuta *et al.*, «Mechanisms of charge-exchange in the $^{12}\mathrm{C}(^{7}\mathrm{Li}, ^{7}\mathrm{Be})^{12}\mathrm{B}$ reaction at the beam energy of 82 MeV», *Nucl. Phys. A* **773**, 187 (2006).

[14] S.Yu. Mezhevych *et al.*, «Elastic and inelastic scattering of $^{14}\mathrm{C} + {}^{11}\mathrm{B}$ *versus* $^{12,13}\mathrm{C} + {}^{11}\mathrm{B}$», *Eur. Phys. J. A* **50**, 4 (2014).

[15] I.J. Thompson, «Coupled reaction channels calculations in nuclear physics», *Comput. Phys. Rep.* **7**, 167 (1988).

[16] Yu.F. Smirnov, Yu.M. Tchuvilsky, «Cluster spectroscopic factors for the p-shell nuclei», *Phys. Rev. C* **15**, 84 (1977).

[17] A.T. Rudchik, Yu.M. Tchuvilsky, *Ukr. Fiz. Zh.* **30**, 819 (1985).

[18] A.T. Rudchik, Yu.M. Tchuvilsky, «The Code DESNA», report KIYAI-82-12 Kiev Institute for Nuclear Researches, 1982.

[19] A.N. Boyarkina, «Structure of the 1p-shell nuclei» report, Moscow State University, 1973.

[20] N. Burtebayev *et al.*, «Measurement and analysis of $^{10}\mathrm{B} + {}^{12}\mathrm{C}$ elastic scattering at energy of 41.3 MeV», *Int. J. Mod. Phys. E* **28**, 1950028 (2019).